Laboratory investigation of performance of a screen type debris-flow countermeasure

A. L. Yifru[a], E. Laache[b], H. Norem[c], S. Nordal[a] and V. Thakur[a]

[a]Geotechnical Division, Department of Civil and Environmental Engineering, NTNU, Trondheim, Norway; [b]Rambøll Norge AS, Kristiansand, Norway; [c]Professor Emeritus at the Department of Civil and Environmental Engineering, NTNU, Trondheim

ARTICLE HISTORY
Compiled May 9, 2018

ABSTRACT
Debris-flows are forms of landslides in mountainous regions that can potentially cause significant damage. Structural countermeasures to mitigate an entire debris-flow may become unrealistically large and expensive. If the flow cannot be stopped completely, one may alternatively consider reducing the impact and velocity of the flow using energy dissipating structures. A debris-flow screen is such countermeasure designed to dissipate energy. A screen is made by parallel grids, with some gap, placed in the direction of the debris-flow on an elevated foundation. This structure acts as a filter for separating water from the saturated debris-flow to reduce its flow energy.

This work presents a laboratory model test investigating the effect of screen length (0.5 m and 1.0 m) and opening width (2 mm, 4 mm and 6 mm) in dissipating the debris-flow energy. The effectiveness of the screens was determined in terms of reductions in the run-out distance and flow velocity. The importance of the screen length and opening width is demonstrated. A hypothesis that the optimum opening size should be close to d_{50} of the solid material seems to be validated. The application of the laboratory observations to the field is indicated based on the energy line and scaling principles.

KEYWORDS
debris-flow, debris-flow screen, countermeasure, laboratory testing, physical modelling

1. Introduction

A debris-flow is a destructive natural hazard that occur in regions with steep or mountainous terrain. Depending on the place and time, debris-flows place human lives and infrastructure in danger. Figure 1 shows a debris-flow that occurred by a steep mountain with an average slope of $\sim 35^\circ$ and an initiation location 425 m above the road level. The total run-out distance is estimated to be 750 m, with a maximum deposition width of 150 m and a thickness of 2 m at the road section. The volume of such a debris-flow is in the order of tens of thousands of cubic metres.

A debris-flow involves a rapid to extremely rapid downhill movement of a mixture of water, soil, gravel and organic matter in a relatively long and steep channelled terrain. Debris-flows significantly affect countries like Norway, which have abundant

CONTACT A. L. Yifru. Email: ashenafi.yifru@ntnu.no

Figure 1. Example of a debris-flow in the coastal areas of Norway [Hunnedalen, Norway - occurred on 2 June 2016]. (Courtesy: Multiconsult and NPRA).

precipitation or water sources and such terrains. These vulnerable countries include Austria, Canada, the Caribbean, China, Colombia, France, Indonesia, Italy, Japan, Nepal, the Philippines, Taiwan, Switzerland, and Venezuela [1].

Because of the constituents of a debris-flow and the irregularity of the terrain where it occurs, its flow mechanism is highly complex and is not fully understood. The existing literature contains numerous studies that attempt to understand the mechanism and behaviours of debris-flow, e.g. ([2–6]); empirical or analytical approaches to quantify the mobility of debris-flow, e.g. ([7–12]); mapping of debris-flow hazard zones, e.g. ([13–18]; investigation of debris-flow triggering causes, e.g. ([19–21]); debris-flow countermeasures, e.g. ([9,22–30]).

Debris-flow countermeasures are preventive methods designed to reduce the existing risk of debris-flows to an acceptable level of residual risk, and they are generally classified into two main categories: structural and non-structural countermeasures [22]. Structural countermeasures are physical barriers or partial obstacles to completely or partly stop the debris-flow. However, non-structural countermeasures are mostly methods focusing on reducing the damage and loss by setting up early warning systems, hazard mapping and land-use zoning.

Structural countermeasures focus on reducing the probability of debris-flow occurrence or their damaging consequences by manipulating their flow course. These types of countermeasures can be applied at the initiation, transportation or even deposition zones of expected debris-flow locations. The potential, working mechanism, and design principles of structural countermeasures such as barriers, baffle and deflection walls have been extensively studied and reported in the literature, i.e. open and closed check dams or generally rigid and flexible barriers [24,25,28,29,31–38], baffle walls [26–28,39,40], deflection and channel-side walls [9,22,41], and debris-flow screens [42–45].

Rigid barriers are those countermeasures designed to fully or partially stop a debris-flow. A sabo dam with a sediment basin is a complete debris-flow stopping counter-

measure that is designed according to peak debris-flow discharge and total volume [23]. The possibility of the sediment storage basin being filled during a single debris-flow event is high. Maintenance of this countermeasure requires excavation of several cubic metres of debris, which is impractical. A closed check dam is a similar kind of countermeasure but smaller in size and it only helps breaking the flow velocity while storing part of the debris-flow at its back. This type of countermeasure is usually designed and constructed sequentially along a stream to prevent bed erosion and to raise the channel bed and reduce the stream gradient [22], which can control debris-flow energy.

Open check dams with steel grids are designed to trap larger-sized boulders from the debris-flow, allowing the rest to pass through with a reduced flow velocity. Open check dams are designed to be self-cleaning from the subsequent stream flows, although most exhibit the deposition of finer sediments at the upstream due to boulders and woody debris interlocking at the grid opening [22,23]. However, open check dams takes approximately 3–10 times longer time to be filled by sediment than the fully blocking dams [22]. A slit dam is another type of open dam that is designed to temporarily retain bed-load, allowing some smaller-sized particles to pass while retaining large boulders with high destructive potential [22]. A channel-side wall and a deflection wall are similar structures that are implemented at different situations and locations. A channel-side wall is implemented to protect stream banks from further erosion and debris overflow. A deflection wall, however, is constructed to direct the debris-flow out of its course and towards areas of low consequence [22].

Another energy-dissipating structure is a baffle wall, which is usually used in combination with rigid barriers and is implemented in several rows, with a systematic staggered arrangement to reduce the debris-flow's impacting force on the downstream rigid barrier. The empirical-approach design of baffle walls is improved using flume model studies that provide the optimum spacing between baffles and between rows of baffles, as well as the ideal baffle height with respect to the flow height of the expected debris-flows [26,27,39]. A debris-flow screen is another countermeasure designed to reduce debris-flow energy [46], and it is usually located at the most upstream position in a system of debris-flow countermeasures, and it has a capacity to retain at least the volume of a debris-flow surge wave [22]. Unlike debris-flow screen that is implemented horizontally across a debris-flow channel, flexible barrier that is made of steel rope is placed vertically and is designed to trap major part of a debris-flow while allowing the water and some of the fine soil particles. Due to successful application of flexible barrier in mitigating rock fall hazards, it has been implemented and tested for its potential in mitigating debris-flows, mainly in Switzerland and Hong Kong [19,24,32,33].

Not many structural countermeasures are used in Norway to mitigate debris-flows; however, deflection walls are widely used for guiding snow avalanches to protect downstream infrastructures and inhabitants. Flexible barriers have also been used to mitigate rock falls in some parts of Norway. In recent years, the destruction of road infrastructures and the interruption of traffic by debris-flow events in Norway have been increasing due to the rapidly changing climate, according to the report from the Norwegian Water Resources and Energy Directorate, NVE [47]. The report explains the strong relation between the changing climate and an increased frequency of debris-flow events in Norway. This gives rise to the need to study and implement appropriate countermeasures for such debris-flows. Check dams and baffle walls are studied for their potential in reducing the run-out distance of debris-flows in a laboratory model [40]. Different combinations of deflection and inclination angles of deflection walls are also tested in the same laboratory model to investigate the run-up height potential of debris-flows [41]. A general guideline in application of various countermeasures to

mitigate debris-flow hazards is given by the Norwegian Public Roads Administration [48].

The south-western and northern parts of Norway are highly susceptible regions for debris-flow-related hazards [49]. These regions have highways that run under the feet of mountains and by the sides of fjords or lakes. Occasionally, debris-flows interrupt traffic, as shown in Figure 1. For such relatively small volume debris-flows, mitigation measures, like energy-dissipating structures and/or guide walls with an underpass at the road section, can be more suitable. At a known location of debris-flow hazard, it might be more economical and easier to implement an energy-dissipating structure to prohibit stream erosion or a small landslide from developing into a debris-flow, assuming the area is accessible for installation and maintenance.

A debris-flow screen is one of such flow energy-dissipating structures, and it can be made from one-directional arrangement of a certain length of steel rods or wooden logs, with a specified gap to separate the water and fine-grained soil from the saturated debris-flow. This study attempts to investigate the applicability of debris-flow screens. As a first step in this direction, physical model tests were conducted to investigate the potential and effectiveness of debris-flow screens. Two screen lengths (0.5 m and 1.0 m) and three opening widths (2 mm, 4 mm and 6 mm) were used to study the flow energy and the run-out distance reductions of a 50 litre (0.05 m^3) debris-flow in a 9 m long and 0.6 m wide flume model. The experiment investigates the optimal opening width and length of debris-flow screen in relation to the d_{50} of the debris(soil) material property.

2. Debris-flow screen

The idea of the debris-flow screen was conceived in Japan in the 1950s to reduce the energy in debris-flows and, thus, contribute to mitigating damage in downstream areas [50]. The main purpose of the debris-flow screen is to separate water from the moving debris. As a result, the pore-water pressure will dissipate from the shearing zone and the rest of the debris-flow mass. In return, the soil particles regain their contact friction and thereby increase shearing resistance of the moving debris [42,45,51]. A schematic representation of a debris-flow screen is illustrated in Figure 2.

Numerous researchers have tested debris-flow screens, and a field trial in the Kamikami-Horisawa Valley, Japan has also been reported in the literature (e.g.[23, 42,43]). The debris-flow screen in the field trial was 20 m long and 10 m wide. The screen grids are made from 0.2 m × 0.2 m square steel tubes that were 8 mm thick and resting on 0.4 m × 0.4 m wide flange beams at a spacing of 0.2 m [42].

Due to their simple construction and cost effectiveness, debris-flow screens have been implemented and used in other countries, including China [44,52] and the Philippines [50,53]. Debris-flow screens have been used to protect mountain roads by installing them in narrow sections of streams where recurrent debris-flows occur.

To study the performance and effectiveness of debris-flow screens, Gonda [42] conducted a small-scale model study with different opening widths on the debris-flow run-out distance, using three different uniform-sized materials of 700 cm^3 volume. The study found that the reduction in run-out distance increases with an increase in the opening width of up to approximately 2 mm. Kim [43], however, investigated three different bed sediments of 13 300 cm^3 volume with three different blocking and opening widths of debris-flow screens. The study showed the effect of opening width percentage in reducing the run-out distance. However, the above two studies used the debris-flow

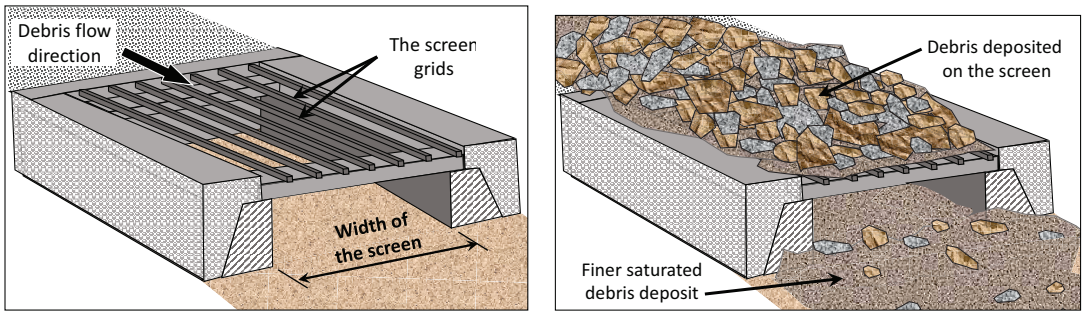

(a) A debris-flow screen structure prior to a debris-flow event.

(b) The debris-flow screen after stopping a granular part of the debris-flow.

Figure 2. Schematic representation of a debris-flow screen's performance.

screen as a deposition area and in all the tests, the debris-flow's mass was retained on the screen.

In real debris-flow cases (as shown in Figure 2), the entire debris-flow volume might not be deposited on the debris-flow screen. Therefore, in the current study, it is interesting to look into the run-out and velocity reduction potential of different screen lengths in combination with different opening widths. The details of the debris-flow's working mechanism are discussed in Section 2.1.

2.1. Working mechanism of a debris-flow screen

The body of a debris-flow surge consist of a water-saturated, muddy, granular slurry liquefied by high pore-water pressure, whereas the front of a debris-flow surge consists of unsaturated, coarse-grained, granular rubble that is pushed from behind by the liquefied slurry [3]. The high pore-water pressure in excess of the hydrostatic water pressure facilitates the high mobility of the debris-flow and is maintained through the entire course of the flow. Savage and Iverson [54] expressed the components of the total normal stress, σ, as a sum of the effective stress between grains, the hydrostatic water pressure and the excess pore-water pressure. A schematic representation of this total normal stress distribution of debris-flow on a solid surface is seen in section A in Figure 3(a) and (b).

Widespread natural decay of pore-water pressure in the flow margin does not contribute to debris-flow deposition, rather it is the grain-contact friction and bed friction concentrations [55]. Major and Iverson [55] showed that the pore-water pressure persisted until the debris-flow was deposited, and then it dissipated significantly during post-depositional sediment consolidation. Therefore, one can introduce a debris-flow screen that helps facilitate the dissipation of pore-water pressure. This results in increasing of the grain-contact friction and grain-bed friction concentration by the sudden removal of the liquid, i.e. dissipation of the pore-water pressure, as schematically shown in Figure 3(a) and (b) in section B.

The energy grade line (energy line) of debris-flow in section A and B can be expressed as the total energy in terms of head, H, which can be given by the Bernoulli equation. Considering an open channel flow situation, the Bernoulli equation of debris-flow just before the beginning of the screen, in section A, can be expressed as:

$$H_A = z_A + h_A + \frac{(v_A)^2}{2g} \tag{1}$$

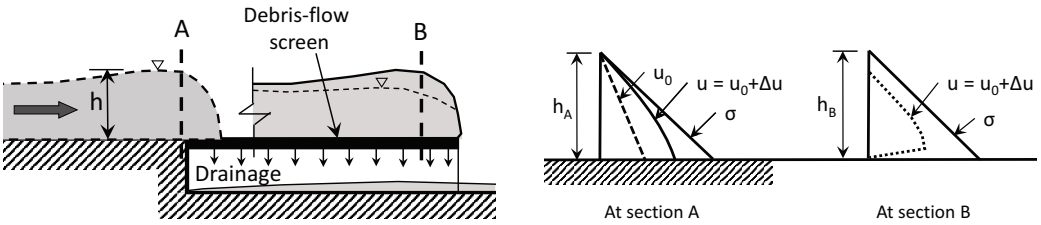

(a) Schematic representation of a debris-flow on a solid surface and on a debris-flow screen.

(b) Total normal stress distribution in solid-liquid mixture: Section A is on a solid surface, and Section B is on a debris-flow screen.

Figure 3. Pore-water pressure development during debris-flow and its dissipation when it hits a screen-type countermeasure.

where H_A is the total head in m; z_A is the elevation of a point from a reference datum in m; h_A is the flowing debris pressure head, which is equal to σ_A/γ in m; σ_A is the total normal stress in kN/m^2; γ is the unit weight of the debris kN/m^3; v_A is the flow velocity and g is the gravitational acceleration. Similarly, the energy head at the end of the screen, in section B, can be expressed as:

$$H_B = z_B + h_B + \frac{(v_B)^2}{2g} \tag{2}$$

The effectiveness of debris-flow screen can be shown by the energy-dissipation factor, E_D, which is expressed as:

$$E_D = 1 - \frac{H_B}{H_A} \tag{3}$$

where $E_D = 0$ represents no energy dissipation, while $E_D = 1$ represents the maximum possible energy dissipation.

2.2. Scaling aspects of the physical modelling

In spite of the disproportionately large effects of viscous shear resistance and cohesion, as well as disproportionately small effects in pore-water pressure in small-scale laboratory model tests, it is also important to systematically study debris-flow by simplifying the complex natural processes in scaled-down laboratory models. The mechanism of dissipation of the pore-water pressure and the hydrostatic water pressure while a debris-flow travels over a screen is yet to be fully understood.

To illustrate the working mechanism and effect of the debris-flow screen, either a field experiment or physical modelling in a laboratory is required. Therefore, this study uses physical modelling in a laboratory to systematically study the effects of a debris-flow screen in reducing a debris-flow run-out distance and flow velocity. Monitoring fluid pressure inside a moving debris can be demanding. Therefore, in this study, the energy dissipation of the debris-flow over a given debris-flow screen will be studied by comparing the energy in the moving debris when entering and leaving the debris-flow screen.

The correct scaling is required when setting up a laboratory physical model to maintain the geometric, kinematic and dynamic similarities of the debris-flow terrain and behaviour. The geometric similarity can be achieved by maintaining the shape by

a linear factor, λ, which can be given as:

$$\lambda = \frac{L_M}{L_F} \tag{4}$$

where λ can be referred to as the linear model scale, which is approximately 1/20 for this study; L_F is any linear dimension in the field (nature); and L_M is any linear dimension on the model.

The kinematic similarity, which is based on velocities, should also have a certain scaling factor to relate between the field and model velocities. To estimate this factor, geometric and dynamic similarities are required. A dimensionless number, called the Froude number (F_r), is used in relating model tests with field cases. It is given by the square root of the ratio between the inertia and gravitational forces of the flow, and it is simplified and shown in Equation 5.

$$F_r = \frac{v}{\sqrt{gh}} \tag{5}$$

where v is the velocity of the moving debris in m/s; g is the gravitational acceleration in m/s^2; and h is the flow height of the moving debris. To conduct a laboratory experiment on debris-flow, the Fr value should be equal to that of the field. However, the resulting Fr for most model tests is observed to be higher than that of a typical debris-flow at the field. From data collected from the field and miniaturised model test measurements, an Fr value less than 2 is seen in real debris-flow cases, while a range of 1.2–12 has been observed in small-scale model tests [56].

Debris-flows generally have velocities between 5 m/s and 10 m/s where the terrain slope angle is close to 20° [48]. NPRA [48] assumes the slope of the energy line to have a gradient between 0.2:1 and 0.3:1 in the run-out zone after the 20° point. The slope angle is an important parameter to fulfil the model-scale laws, which should be maintained when building a laboratory model for debris-flow study.

3. Physical Modelling

3.1. The model set-up

The flume model used for this study is 9 m long and has two parts: a run-out channel and a deposition area. The run-out channel has two inclinations, 23° and 14° slopes, and it is 0.6 m wide and 0.3 m high. The deposition area is 3.6 m long and 2.5 m wide, with a 2° inclination. Figure 4 provides a schematic representation of the model.

Two identical wooden crates (boxes), measuring 0.9 m × 0.6 m × 0.8 m, were used for containing the debris-flow material. One crate was used for releasing the debris, and the other is used for collecting it before and after each test. The debris-flow screen was placed at the end of the run-out channel. The flume model was instrumented with two flow-height sensors before and after the debris-flow screen. The first sensor was used to measure the flow height in the run-out channel, while the second measured the deposition thickness at the deposition area. Three video cameras were used to capture the flow behaviour, in which Cam-1 was placed above the run-out channel, Cam-2 was placed above the deposition area and Cam-3 was placed at the front of the flume model. Cam-1 was used to record the debris-flow's behaviour when it interacted with the debris-flow screen.

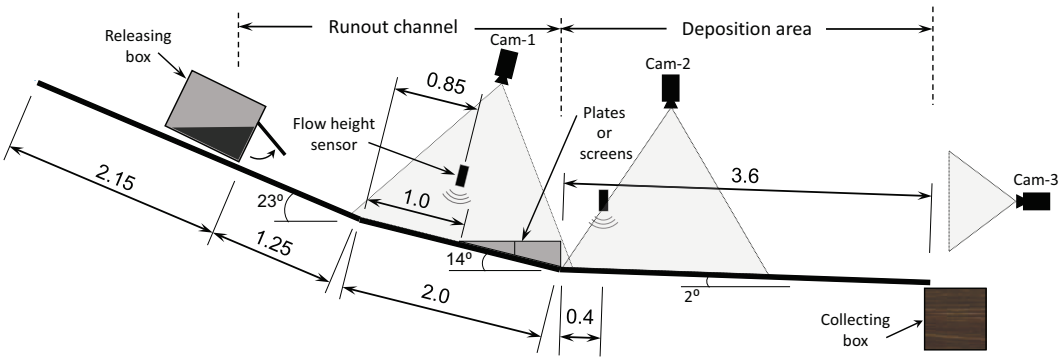

Figure 4. The flume model, placement of debris-flow screens and instrumentation. All linear dimensions are in metres.

3.2. Methodology

A 100 kg soil-water mixture was prepared by mixing 80 kg of soil and 20 kg of water to simulate a saturated debris-flow. These weighted amounts of soil and water were added to the releasing box and were then thoroughly mixed. The soil–water mixture corresponded to a total of 50 litres (0.05 m^3) of fully saturated debris material with a solid concentration of $C_s = 60\%$ by volume. This saturated debris represents well-developed and fast-moving debris-flow material upon release. In the experiments, the releasing mechanism simulated a dam break by releasing the whole mass at once, as the focus of the study was to investigate the behaviour of a well-developed debris-flow interaction with different debris-flow screen types.

To conduct a given test, the releasing box with the saturated debris material was lifted by crane and placed on the top end of the run-out channel, as shown in Figure 4. Before releasing the debris mass from the box, video recording started in all cameras, and the flow-height sensors were checked. The debris material was then thoroughly mixed using a hand mixer to create a well-mixed, less-segregated debris-flow upon release. Finally, the gate was opened, and the saturated debris was released.

Two debris-flow screen lengths (0.5 m and 1.0 m) and three screen opening widths (2 mm, 4 mm and 6 mm) were chosen to be tested. The screens were made by the systematic arrangement of rectangular steel rods with a cross-section of 10 mm × 15 mm, using spacers 2 mm, 4 mm and 6 mm in size (see Figure 5(b)). Figure 5(a) shows the placements and starting point of these screens. The starting point of the screens, which is considered as a reference point for measuring the debris-flow's run-out distance, is 2.25 m away from the releasing box and 1.0 m before the start of the deposition area (see Figure 4). In addition, two scenarios that represent only the terrain alteration of the screens are included and used as reference tests, and they are made from 0.5-m- and 1.0-m-long solid plates in which their opening widths are referred to as zero.

After each test, the run-out distance (with reference point 'x' in Figure 5(a)), maximum deposition width and maximum deposition thickness of the soil in the deposition area were recorded. In addition, the maximum deposition thickness on the debris-flow screen was recorded. After taking all the important measurements and representative photos, soil samples from selected tests were taken from different parts of the flow area to evaluate how the grain size distribution of the debris material changed from the original released material. Finally, the model was cleaned and made ready for the

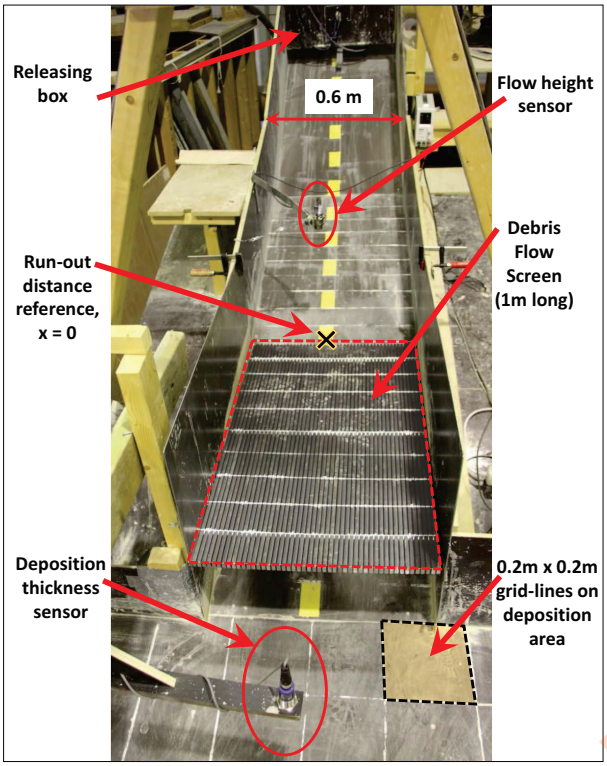

(a) The run-out channel and partial view of the deposition area (photo from Laache [57]).

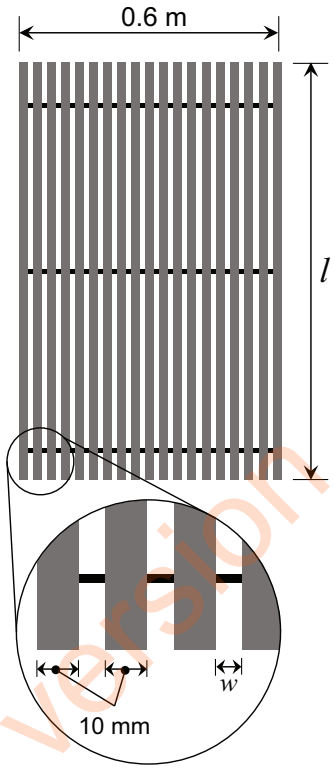

(b) A schematic detail of the debris-flow screen: l is 0.5 m or 1.0 m and w is 2 mm, 4 mm and 6 mm.

Figure 5. Details and measurements of the run-out channel, the screens and the deposition area.

next test.

3.3. Test plan

The test plan is given in Table 1. The 24 tests are named based on the various scenarios and are given the code *'s-l-w-n'*, where s is scenario, l is the length of a screen in m, w is the width of a single opening on a screen in mm, and n is the scenario repetition number. Each scenario was repeated three times and numbered as $n = 1$, 2 and 3. The opening percentage is the percentage ratio of the cumulative opening and the width of the screen.

3.4. The test material

The debris material used for this test is a sandy soil with a grain size property of $d_{max} = 8.0\,\text{mm}$, $d_{90} = 6.0\,\text{mm}$, $d_{50} = 1.8\,\text{mm}$ and $d_{10} = 0.11\,\text{mm}$. The grain size distribution (GSD) of the sand is given by Figure 6. The coefficient of uniformity is $C_u = 25$, and the coefficient of curvature is $C_c = 1.96$, which indicates a well-graded material. The specific gravity of the soil is 2.71 at $20°c$. This GSD was maintained without any significant variation throughout the tests.

Table 1. Test plan and description of dimensions of the debris-flow screens used.

Test Number	Test Name	Screen length [m]	Screen opening [mm]	Screen opening [%]	Test Number	Test Name	Screen Length [m]	Screen opening [mm]	Screen opening [%]
T1	S-0.5-0-1				T13	S-0.5-4-1			
T2	S-0.5-0-2	0.5	0	0	T14	S-0.5-4-2	0.5	4	29
T3	S-0.5-0-3				T15	S-0.5-4-3			
T4	S-1-0-1				T16	S-1-4-1			
T5	S-1-0-2	1.0	0	0	T17	S-1-4-2	1	4	29
T6	S-1-0-3				T18	S-1-4-3			
T7	S-0.5-2-1				T19	S-0.5-6-1			
T8	S-0.5-2-2	0.5	2	17	T20	S-0.5-6-2	0.5	6	38
T9	S-0.5-2-3				T21	S-0.5-6-3			
T10	S-1-2-1				T22	S-1-6-1			
T11	S-1-2-2	1	2	17	T23	S-1-6-2	1	6	38
T12	S-1-2-3				T24	S-1-6-3			

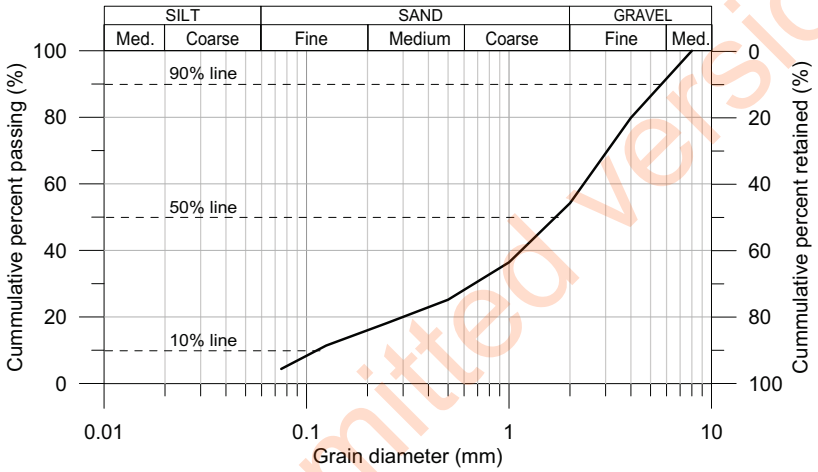

Figure 6. Grain size distribution of the test material.

4. Results

These results are from the experiment made for a Master's thesis by Laache [57], and are re-analysed by the first author. The run-out distance (L_{FL}), maximum width of deposition (B), maximum upstream flow height (h_{Max}), maximum deposition thickness on the screen (t_u) and downstream at the deposition area (t_d), and average front-flow velocity at the beginning (v_A) and the end (v_B) of a screen were recorded for all 24 tests and are summarised in Table 2. Tests T1 to T6 are the reference tests without debris-flow screens, where solid plates of 0.5-m- and 1.0-m-long were used. Tests T7-T24 were conducted using 0.5-m- and 1.0-m-long screens with three opening sizes, i.e. 2 mm, 4 mm and 6 mm. The reference tests were used as the benchmark to evaluate the performance of the debris-flow screens. The model geometry was identical in each test. Therefore, changes in the debris-flow run-out distance and flow velocity are attributed to the debris-flow screen.

The flow-front velocity was measured by analysing the Cam-1 video using Tracker (Tracker v4.11.0), a video processing software. Due to the homogeneous-looking flow of the debris-flow's body and tail, only the flow-front was tracked to compute velocity. In

Table 2. Summary of the test results (Based on data from Lacche [57]).

Test Number	Test Name	L_{FL} [m]	B [m]	h_{Max} [cm]	t_u [cm]	t_d [cm]	v_A [m/s]	v_B [m/s]
T1	S-0.5-0-1	2.35	0.90	3.20	3.35	1.90	2.63	2.23
T2	S-0.5-0-2	2.60	0.87	3.40	2.49	1.70	2.28	1.73
T3	S-0.5-0-3	3.05	1.12	5.40	1.44	1.60	2.00	1.80
T4	S-1-0-1	2.65	1.08	3.50	4.39	1.00	2.63	1.97
T5	S-1-0-2	2.75	1.08	4.90	2.61	0.90	2.47	1.97
T6	S-1-0-3	2.10	0.98	4.00	3.83	1.40	2.87	2.80
T7	S-0.5-2-1	1.95	0.66	3.50	7.71	1.20	3.13	2.57
T8	S-0.5-2-2	1.80	0.98	4.00	5.64	1.30	2.63	1.65
T9	S-0.5-2-3	2.28	0.90	3.20	3.81	1.30	2.93	2.37
T10	S-1-2-1	0.95	0.60	3.60	6.78	0.80	3.03	0.00
T11	S-1-2-2	0.90	0.60	3.40	5.62	0.30	-	-
T12	S-1-2-3	0.90	0.60	3.70	5.89	0.40	2.67	0.43
T13	S-0.5-4-1	2.25	1.18	3.90	5.20	2.00	3.10	2.27
T14	S-0.5-4-2	2.50	1.08	3.50	3.75	1.70	2.90	2.43
T15	S-0.5-4-3	2.95	1.02	3.90	5.36	1.60	2.77	1.83
T16	S-1-4-1	0.75	0.60	3.70	5.40	0.40	-	-
T17	S-1-4-2	1.00	0.60	3.10	4.22	0.70	2.82	0.57
T18	S-1-4-3	1.00	0.60	3.20	5.07	0.30	3.08	1.10
T19	S-0.5-6-1	2.40	0.85	4.90	6.34	1.20	2.23	1.53
T20	S-0.5-6-2	3.00	1.00	3.60	3.70	1.10	3.20	2.17
T21	S-0.5-6-3	2.50	0.70	3.40	6.17	1.30	2.77	1.63
T22	S-1-6-1	0.90	0.60	4.30	4.86	0.80	2.77	0.10
T23	S-1-6-2	0.90	0.60	3.50	4.39	0.70	2.87	0.40
T24	S-1-6-3	0.90	0.60	4.30	5.85	0.90	2.90	0.50

many of the model test cases, the flow-front velocity was non-uniform across the width of the flow channel because of flow surges. As a result, the average flow-front velocity is computed by considering velocities at the left, centre and right of the flow. The values presented in Table 2 as v_A and v_B are the average approach and the average exit-velocities to and from a debris-flow screen, respectively. Figure 7 presents the flow-front velocities of six representative tests from each scenario group, except for the two reference test scenarios. This is due to limitations of the output video recordings that only the v_A and v_B values were computed and given in Table 2.

Two distinguishing parts of the debris deposit are observed. The first is water mixed with very fine soil particles that continued to flow and ended up in the collecting box. The second is the solid debris that accumulated in the deposition area or on the screen. The L_{FL} and B measurements given in Table 2 are for the solid debris. The photos showing the final deposition shape, along with L_{FL} and B of the four representative tests, are presented in Figure 8. This figure illustrates how the debris material flowed, spread and segregated in the deposition area when using the 0.5-m-long plate and screens.

From the upstream flow-height sensor, variations in the average flow heights with time for all the tests are given in Figure 9. For each test, two peak values were extracted from a respective plot. The first peak represents the h_{Max} while the second, stabilized and horizontal line represents t_u, which are given in Table 2.

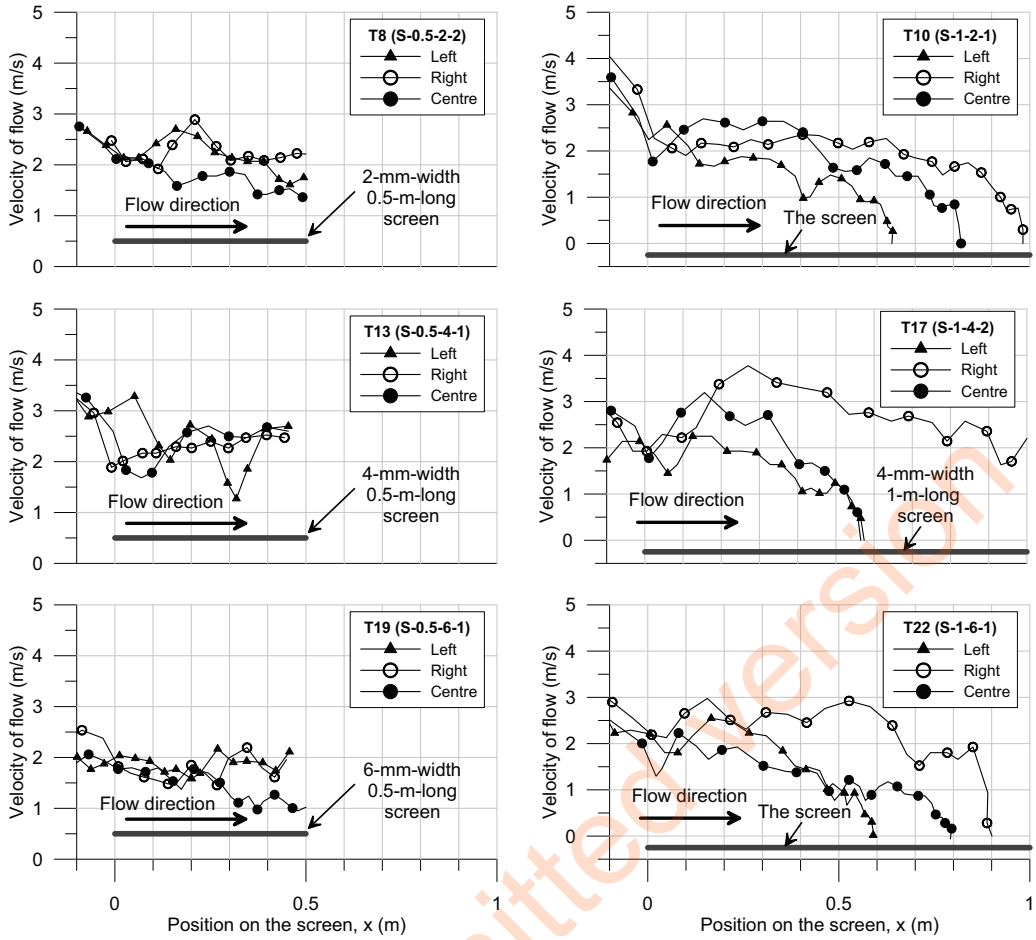

Figure 7. Representative plots showing the flow-front velocities at the left, centre and right sections of the run-out channel over the 0.5-m- and 1-m-long screens; for 2 mm, 4 mm and 6 mm opening widths from top to bottom.

5. Discussion

The reference test results from T1 to T6 will be used as a benchmark for discussing the performance of the debris-flow screens. The average run-out distance, L_{FL}, for the 0.5-m-long reference test (T1–T3) is 2.67 m, with a standard deviation of 0.35 m, while for the 1.0-m-long reference test (T4–T6), the average L_{FL} became 2.5 m, with a standard deviation of 0.35 m. As expected, the resulting L_{FL} is found to be shorter for the longer slope-alteration length than the shorter.

The average value of the maximum deposition width, B for the 1.0-m-long reference test, is found to be slightly wider than that of the 0.5-m-long reference test. A wider B can be an indication of slower flow-front in the deposition area, which forced the flow-tail to spread side ways, causing a shorter L_{FL}. Similarly, a lower average upstream deposition, t_u, and a higher average downstream deposition, t_d, were observed in the case of the 0.5-m-long plate than for the 1.0-m-long plate. The average t_u for both reference tests can be seen in Figure 9 between $t = 4s$ and $t = 5s$.

In both cases, the flow velocities were decreased at the end of the plates when compared to the velocity at the beginning of the plates. The average flow-front velocity decrease was observed to be in the order of 15%, which can be considered as a channel

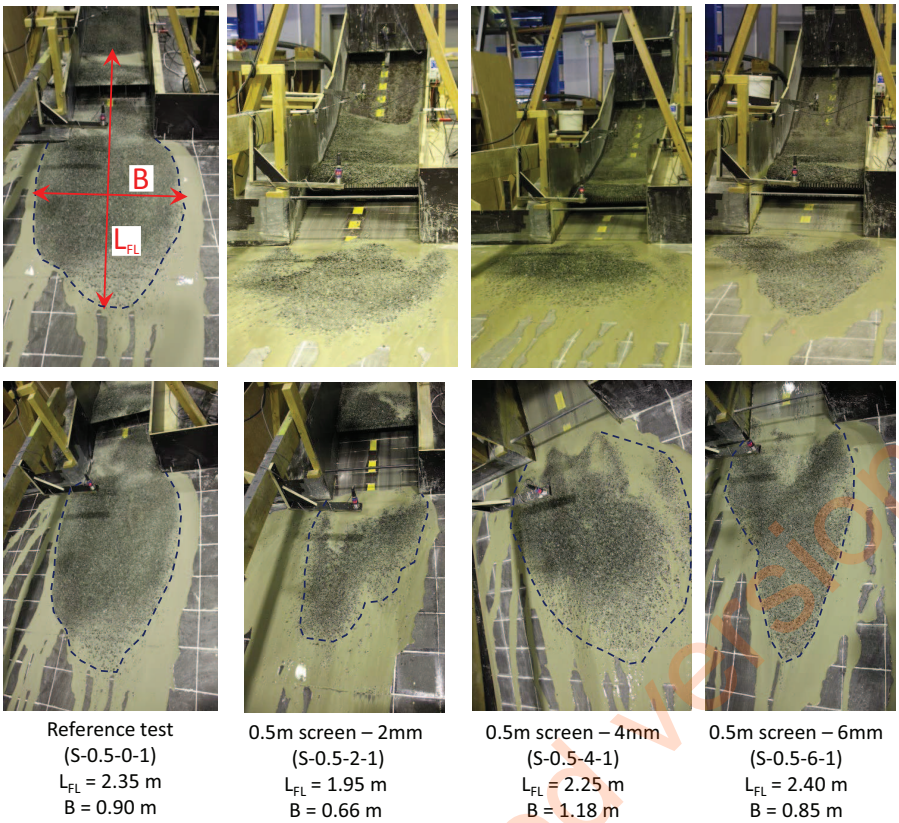

Figure 8. Photos showing deposition pattern and run-out distance of selected tests from 0.5-m-long cases (Photos from Laache [57]).

alteration contribution.

5.1. The run-out distance

The recorded L_{FL} are plotted against the opening width of the screen for each length in Figure 10. The plot shows the average L_{FL} along with the lower- and upper-bound values represented by error bars. The lower- and upper-bound values are those given in Table 2.

The average L_{FL} when using the 0.5-m-long screen is observed to decrease to 2.01 m with the provision of a 2 mm opening width. However, the average L_{FL} showed no significant change from the reference test when using 4 mm and 6 mm screen opening widths (T13–T15 and T19–T21). The respective average L_{FL} were 2.57 m and 2.63 m, which are not far from the reference average of $L_{FL} = 2.70$ m. One possible reason for these relatively longer L_{FL} values may be the mixing of the sufficiently fast liquid and solid fractions filtered through the screen with the material that jumped over the screen.

The 1.0-m-long screen is observed to be sufficient for the debris-flow volume, as it retains almost the entire granular part of the test material. The L_{FL} were also found to be relatively consistent, with an average value of around 0.9 m for all the three opening widths. All were less or equal to the total screen length. However, some solid fractions that had filtered through the 4 mm and 6 mm screens were observed in the

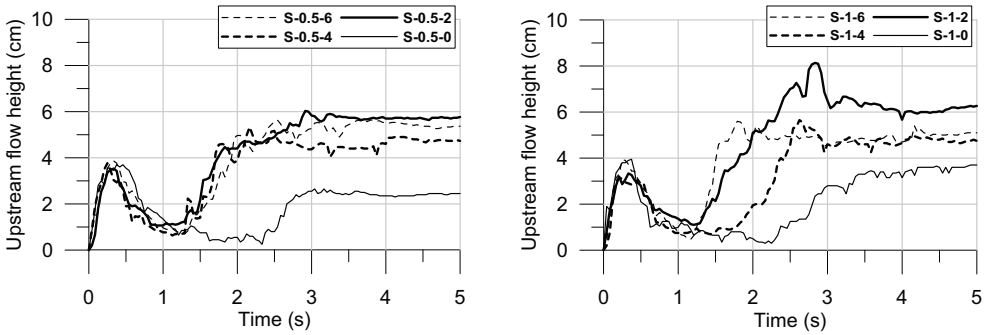

(a) Average flow heights when using a 0.5-m-long plate and screen.

(b) Average flow heights when using a 1.0-m-long plate and screen.

Figure 9. Average flow height variation with time at the upstream of the countermeasures.

deposition area. In addition, for test T17 and T18 of the 4 mm opening screens in particular, a saturated surge on one side of the channel was observed to travel the whole length of the screen, which produced a 1-m-long L_{FL}.

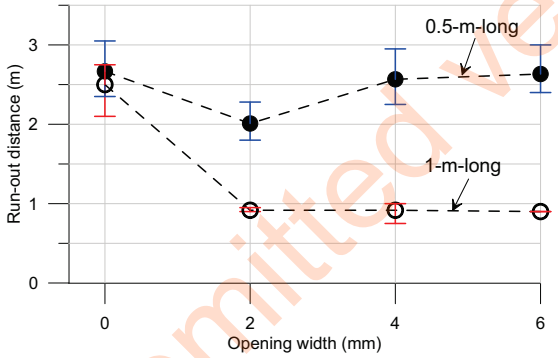

Figure 10. Run-out distance with respect to the opening widths of the 0.5-m- and 1-m-long screens

5.2. Flow velocity

The average flow velocities recorded approaching, v_A, and exiting, v_B, the respective plate or screen are given in Table 2. As expected, the average v_A is consistent and between 2.65 m/s and 2.95 m/s, except some outliers were observed in T3 and T20 with very low and very high velocities. This variation is a result of different surges observed in different sections of the flow channel, as shown in Figure 7.

Although average velocity reductions are observed due to the terrain alteration in the reference tests and the water-draining effect in the screens, the value of v_B was affected by small surges of highly-saturated debris mass. Some of the v_B values of the 1-m-long screen shown in Table 2 are non-zero; this is the effect of a small flow-front part, either in the left or right of the channel, which shoots until the end of the screen. In the cases of T17 and T18, the average exit-velocity value was as high as 1.1 m/s. However, the average exit velocities when using 0.5-m-long screen vary, and more will be discussed based on the energy dissipation.

5.3. Maximum flow height and deposition thickness

Like the approach flow velocity, v_A, the maximum flow height, h_{Max}, recorded at the upstream sensor was expected and observed to be uniform. The average h_{Max} was around 3.5 cm (see Figure 9). Some outliers were observed in T3, T5 and T19 that gave h_{Max} between 4.9 cm and 5.4 cm. These thick flow heights are due to some saturated frozen (lumped) masses that were not fully mixed with the rest of the fluidized debris.

In discussing the upstream deposition thickness, t_u, Figure 9 shows that the flow height increases after the $t \approx 1.5s$ mark. This is due to the damming effect from the decelerating flow-front, which is the first to lose its water content. As the flow proceeds, the amount of dry flow-front increases, as well as the grains' resistance through grain-contact friction and grain-bed friction, while the flow-tail still pushes. However, after a short time ($\sim 1s$), the major part of the flow-front stops completely and acts as a dam to halt the entire flow-tail, including the remaining liquid. After the debris mass was deposited on the debris screen, the liquid held at the back of the debris-dam continued to drain slowly through the mass and the screen. In some tests, a turbulent flow behind the debris-dam was observed, and one of them is visible on the plot of (S-1-2) in Figure 9(b).

The resulting average t_u vary between 4.7 cm and 6.1 cm for both screen lengths, whereas for the reference tests, the average t_u was recorded as 2.5 cm and 3.6 cm for the 0.5-m- and 1-m-long plates, respectively. The average t_u almost doubled from their respective reference test results when using the 2 mm opening width (T7–T12), while a relatively lesser increase was seen when using 4 mm and 6 mm opening widths.

In comparing the downstream deposition thickness t_d, the 1-m-long screens gave an average t_d thickness of less than 1 cm, as there is no significant debris mass in the deposition area. When using the 0.5-m-long screen, the lowest average t_d were observed during the 2 mm and 6 mm opening widths, while a similar average t_d was recorded as that of the reference test when using the 4 mm opening width. This can also be considered as a measure for the decrease in the amount of the debris passing the screen. Therefore, all opening widths from the 1-m-long screen, and the 2 mm and 6 mm opening widths from the 0.5-m-long screen were found to reduce the downstream deposition thickness by up to 33%.

5.4. Effectiveness of the screens

5.4.1. Run-out distance reduction

Effectiveness of the screens can be evaluated using the percentage decrease in average L_{FL} in comparison with the average L_{FL} of the respective reference test. This calculated effectiveness is presented in Figure 11 and plotted against the opening width for each screen length.

The 2 mm opening width reduced the average L_{FL} observed in the reference tests of 1 m and 0.5 m by 63% and 25%, respectively. For the 0.5-m-long screen, this is the highest percentage reduction on average L_{FL}, while the 1-m-long screen keeps almost the same percentage reduction for all opening widths. However, the percentage decrease in average L_{FL} for the 4 mm and 6 mm opening widths in the 0.5-m-long screen case are less than 4% and 1.3%, respectively. The reason for these small percentage reductions is the result of the fast-moving water and soil fractions passing through the screen and mixing with the debris that jumped over the screen to travel longer. The resulting percentage reduction when using the 2 mm opening width for both screen

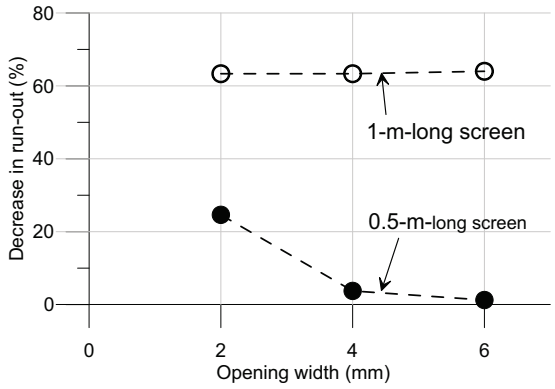

Figure 11. Percentage run-out distance reduction of the debris-flow screen based on length and opening width, with respect to the reference run-out distances.

lengths can be an indication of an interesting relationship between the opening width and the $d_{50} = 1.8\,\text{mm}$ of the testing material used.

A similar experiment done in Kyoto, Japan, by Kim [43], showed assessment of the effectiveness of the screen-type debris-flow countermeasure based on the percentage of the ratio between the cumulative opening width and the total width of the screen. The screen was, at the same time, used as a deposition area for the tested material, which makes it suitable to compare it with the 1-m-long screen used in this study. Therefore, the data from Kim [43] with $d_{50} = 1.78\,\text{mm}$ is plotted against the data from the present study and given in Figure 12. The blocking width of the screens, in the present study, is a constant 10 mm, while Kim [43] varied it along with the opening widths, which might explain the slight variations in the results when it comes to the low-percentage openings of 17% and 29%. The 0.5-m-long screen case is not comparable, as the debris material run beyond the screen.

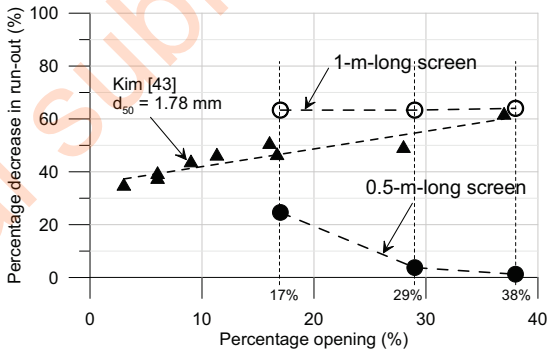

Figure 12. Comparison of percentage opening versus percentage run-out distance reductions with data from Kim [43].

5.4.2. Energy dissipation

Energy dissipation potential is another aspect for evaluating the effectiveness of a countermeasure. Because of the horizontally aligned provision of the debris-flow screens and an extremely low-pressure head compared to the velocity head, the energy dissipation between the beginning and end of each screen will be assessed by the velocity head

term only i.e. $v^2/(2g)$, (from Equation 1 and 2). Then Equation 3 is simplified as:

$$E_D \approx 1 - (\frac{v_B}{v_A})^2 \tag{6}$$

where v_A and v_B represent the average velocities given in Table 2.

Figure 13 shows the average percentage energy dissipated in each case. In both the 0.5-m- and 1.0-m-long screen cases, the major amount of energy is dissipated when using the 2 mm opening width. When using the 4 mm and 6 mm opening widths, no significant increase in energy dissipation beyond what is obtained by the 2 mm opening width is observed in the case of the 1.0-m-long screen. However, a gradual increase in energy dissipation is observed when using the 0.5-m-long screen. In the case of the 4 mm opening width and 1-m-long screen, the energy dissipation is seen to be small and out of the data trend. This might be attributed to the high flow velocity observed at the end of the screen by some small portion of the debris-flow front.

Generally, the average percentage energy dissipation presented in Figure 13(b) implies that, without the contribution of the terrain alteration, the 1-m-long debris-flow screen can reduce the flow energy up to 70%, while the 0.5-m-long screen is able to reduce the flow energy between 25% and 50%.

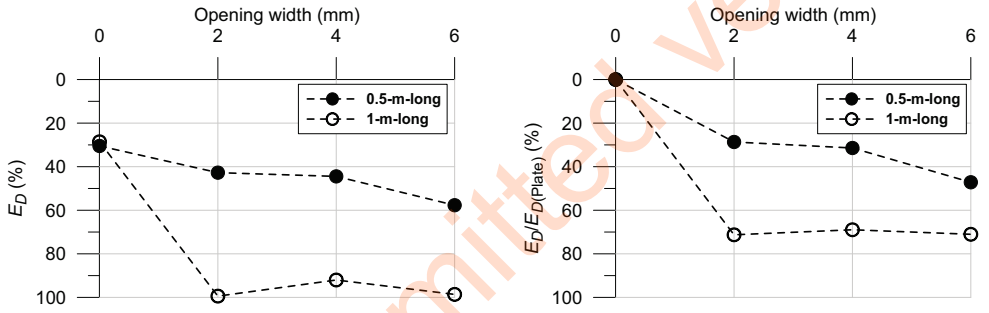

(a) Percentage of energy-dissipation factor with opening width.

(b) Percentage energy-dissipation with respect to energy-dissipation factor by terrain alteration (from reference tests).

Figure 13. Illustration of energy-dissipation factor for evaluating effectiveness of debris-flow screen-types.

5.5. Segregation of the debris material

Soil samples from the deposition area and from the top of the countermeasures were collected to study the segregation or change in grain size distribution of the original debris-flow material. The selected tests are T7 (S-0.5-2-1), T13 (S-0.5-4-1) and T19 (S-0.5-6-1).

The samples that are taken from the top of the screen were collected from the end of the screens because the material deposited in the middle or at the back of the screen is affected by the debris-tail (subsequent flow surges), while the front material is interacted fully with the screen to show the effect of the screen.

A sample GSD plot (Figure 14) from T7 (S-0.5-2-1) shows that the material accumulated on the screen was coarser than the original material, while finer materials were observed in the deposition area. Table 3 shows a comparison using the d_{50} values of the tested samples. The values given in the table demonstrate that the screens can

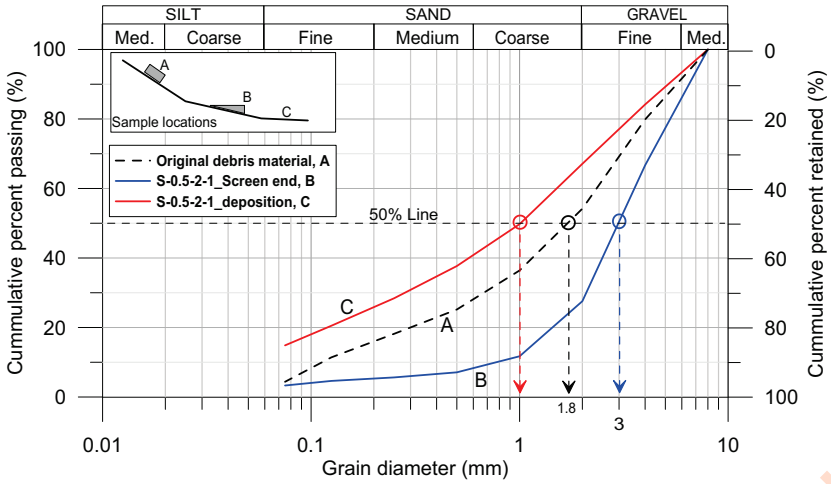

Figure 14. Change in grain size distribution (GSD) of the debris-flow material on the screen and at the deposition area.

retain the major coarse part of the debris-flow. This also shows that debris-flow screens are not only breaking the flow but also have the potential to retain coarser debris that might have significant destructive powers.

Table 3. Values of d_{50} for the samples at deposition and on the 0.5-m-long screen

Test number	Scenario	d_{50} screen end	d_{50} deposition area
T7	S-0.5-2-1	3.0	1.0
T13	S-0.5-4-1	4.2	1.4
T19	S-0.5-6-1	2.7	1.6

In general, the performance of the debris-flow screen with respect to the opening width can be discussed in light of the soil material grain size property, d_{50}. The d_{50} of the test material is 1.8 mm. In the case of the 4 mm and 6 mm opening widths, the d_{50} values in the deposition area are found to be greater than that of the 2 mm cases. This indicates that the mass in the deposition area is not only the soil that is pushed over the screen but also the soil that is filtered through the openings along with the muddy liquid. This phenomenon is observed in the case of the 1-m-long screen as well, where some soil grains escaped through the 4 mm and 6 mm screens.

If not for the frictional force between the soil grains, 6 mm and 4 mm opening widths could allow 94% and 80% of the debris solids, respectively, while the 2 mm opening width could allow 54% of the debris solids through the openings of the screen. This gives another perspective on why the first two allowed some soil fractions and were less effective than the latter. This might be an interesting observation that relates the debris material property, d_{50}, with the opening width on the performance of debris-flow screens. Thus, this observation during the use of the 2 mm opening width in both screen lengths may contribute to the possible use of d_{50} as a design criterion for the optimal opening of debris-flow screens.

5.6. Scaling effect

In laboratory model studies of debris-flows, the slope of the energy line is one of the important model scale laws that must be maintained. According to NPRA [48], the slope of the energy line is expected to fall between 0.2:1 and 0.3:1. Three model calibration tests, without any structure in the flume channel and deposition area, were carried out, and the slope of the average energy line was 0.22:1, satisfying the requirement [57].

From the recorded maximum flow heights and flow velocities, the Fr values were calculated, and the maximum and minimum values were 5.5 and 2.75 for test numbers T3 and T18, respectively. This ensures that the Fr of the model test results are with in the range given as $1.2 < Fr < 12$ by Huebl et al. [56]. However, a typical debris-flow in nature has an Fr value around 2.

The scaling effect can be discussed in terms of the geometric linear scale λ. The model is assumed to have an approximate linear scale of $\lambda = 1/20$. According to the linear scale factor, the initial volume used in the model, i.e. $0.05\,\mathrm{m}^3$, will give an approximate scaled-up volume of around $400\,\mathrm{m}^3$. Such volume can be related to a small debris-flow, which can be said that a 20-m-long debris-flow screen could dissipate a major part of the debris-flow energy. The Kamikami-Horisawa Valley field experience on debris-flow screen [23,43,58] can give an overview of the size and volume of flow along with the tested screen length.

Encouraging results are found in the model tests. A comparison of these results with field trial in a controlled condition will consolidate the findings. The optimal length of debris-flow screen with different opening widths shall be tested with different flow discharges and volumes. The effect of multiple surges on debris-flow screen performance should also receive close attention.

6. Conclusion

This work attempts to investigate the debris-flow screen on a laboratory model for its potential to dissipate the flow energy of debris-flows. The assessment was done by comparing the effects of different lengths and opening widths of the debris-flow screen on the resulting run-out distances, flow velocities, flow heights and deposition thicknesses.

The 1-m-long debris-flow screen is found to be sufficient to halt the flow of the entire debris-flow volume regardless of the opening width. However, the 4 mm and 6 mm opening widths, which are widths greater than the d_{50} size of the debris-flow material, are found to allow some solid fractions through their openings along with the draining water.

A general observation about the 0.5-m- and 1-m-long debris-flow screens is that the run-out distance and flow velocity decreases with an increase in screen length. However, among the three screen opening widths, the 2 mm ($\approx d_{50}$) opening width was found to be optimal regarding reducing both the run-out distance and flow velocity of the debris-flow. A further increase in the opening width exhibits a relatively small improvement in the reduction of run-out distance and flow velocity.

Further study on different screen lengths and opening widths with varying debris-flow volume will add to this result and consolidate the interesting relationship found between d_{50} and the screen opening width in flow mobility reduction. In addition, validation from a field experiment will be vital to develop robust design criteria for an

effective debris-flow screen.

Acknowledgement

The Norwegian Public Roads Administration, NPRA, financially supported this study under the E39 ferry-free highway project, and the study was conducted in close cooperation with the Klima2050 project. The authors would like to thank Frank Stæhli and Tage Westrum, for building the screens and the plates, and Geir Tesaker for operating the crane during the experiment.

References

[1] Takahashi T. Debris flow: mechanics, prediction and countermeasures. London (UK): CRC Press; 2014.
[2] Takahashi T. A review of japanese debris flow research. Int J of Eros Cont Eng. 2009; 2(1):1–14.
[3] Iverson RM. The physics of debris flows. Rev Geophys. 1997;35(3):245–296.
[4] Iverson RM. Debris-flow mechanics. In: Jakob M, Hungr O, editors. Debris-flow hazards and related phenomena. Berlin, Heidelberg: Springer; 2005. p. 105–134.
[5] Iverson RM, Logan M, LaHusen RG, et al. The perfect debris flow? aggregated results from 28 large-scale experiments. J Geophys Res-earth. 2010;115.
[6] Viccione G, Genovese M, Rossi F, et al. Physical modelling of laboratory debris flows by using the sodium carboxymethylcellulose (na-cmc). WSEAS Trans Fluid Mech. 2015; 10:163–173.
[7] Hungr O, Morgan GC, Kellerhals R. Quantitative-analysis of debris torrent hazards for design of remedial measures. Can Geotech J. 1984;21(4):663–677.
[8] Rickenmann D. Empirical relationships for debris flows. Nat Hazards. 1999;19(1):47–77.
[9] VanDine D. Debris flow control structures for forest engineering. Victoria (BC): Res Br BC Min For.; 1996. Work Pap. 08/1996.
[10] Scheidl C, Rickenmann D. Empirical prediction of debris flow mobility and deposition on fans. Earth Surf Proc Land. 2010;35(2):157–173.
[11] Federico F, Cesali C. An energy-based approach to predict debris flow mobility and analyze empirical relationships. Can Geotech J. 2015;52(12):2113–2133.
[12] Devoli G, De Blasio FV, Elverhi A, et al. Statistical analysis of landslide events in central america and their run-out distance. Geotech Geol Eng. 2009;27(1):23–42.
[13] Sandersen F. The influence of meteorological factors on the initiation of debris flows in norway. In: Matthews JA, Brunsden D, Frenzel B, et al., editors. Rapid mass movement as a source of climatic evidence for the Holocene: Palaeoclimate Research; Vol. 19; Gustav Fischer Verlag, Stuttgart; 1997. p. 321–332.
[14] Glade T. Linking debris-flow hazard assessments with geomorphology. Geomorphology. 2005;66(1):189–213.
[15] Fischer L, Rubensdotter L, Sletten K, et al. Debris flow modeling for susceptibility mapping at regional to national scale in norway. In: Proceedings of the 11th International and 2nd North American Symposium on Landslides; 2012 Jun 03-08; Alberta, Canada; 2012. p. 3–8.
[16] Meyer NK, Dyrrdal AV, Frauenfelder R, et al. Hydrometeorological threshold conditions for debris flow initiation in norway. Nat Hazard Earth Syst. 2012;.
[17] Meyer NK, Schwanghart W, Korup O, et al. Estimating the topographic predictability of debris flows. Geomorphology. 2014;207:114–125.
[18] Devoli G, Strauch W, Chvez G, et al. A landslide database for nicaragua: a tool for landslide-hazard management. Landslides. 2007;4(2):163–176.

[19] Wang G, Sassa K. Factors affecting rainfall-induced flowslides in laboratory flume tests. Geotechnique. 2001;51(7):587–599.
[20] Blijenberg HM. Application of physical modelling of debris flow triggering to field conditions: Limitations posed by boundary conditions. Eng Geol. 2007;91(1):25–33.
[21] Bacchini M, Zannoni A. Relations between rainfall and triggering of debris-flow: case study of cancia (dolomites, northeastern italy). Nat Hazard Earth Syst. 2003;3(1-2):71–79.
[22] Huebl J, Fiebiger G. Debris-flow mitigation measures. In: Jakob M, Hungr O, editors. Debris-flow hazards and related phenomena. Berlin, Heidelberg: Springer; 2005. p. 445–487.
[23] Mizuyama T. Structural countermeasures for debris flow disasters. Int J Eros Control Eng. 2008;1(2):38–43.
[24] Ashwood W, Hungr O. Estimating total resisting force in flexible barrier impacted by a granular avalanche using physical and numerical modeling. Can Geotech J. 2016; 53(10):1700–1717.
[25] Bugnion L, Bötticher A, Wendeler C. Large scale field testing of hill slope debris flows resulting in the design of flexible protection barriers. In: Koboltschning G, Hübl J, Braun J, editors. 12th Congress Interpraevent; 2012 Apr 23-26; Grenoble; 2012. p. 59–66.
[26] Choi CE, Ng CWW, Song D, et al. Flume investigation of landslide debris-resisting baffles. Can Geotech J. 2014;51(5):540–553.
[27] Ng CWW, Choi CE, Song D, et al. Physical modeling of baffles influence on landslide debris mobility. Landslides. 2015;12(1):1–18.
[28] Ng CWW, Choi CE, Su AY, et al. Large-scale successive boulder impacts on a rigid barrier shielded by gabions. Can Geotech J. 2016;53(10):1688–1699.
[29] Wendeler C, McArdell B, Rickenmann D, et al. Field testing and numerical modeling of flexible debris flow barriers. In: Ng CWW, Zhang LM, Wang YH, editors. 6th ICPMG; 2006 Aug 4-6; Hong Kong; 2006.
[30] Scheidl C, Chiari M, Kaitna R, et al. Analysing debris-flow impact models, based on a small scale modelling approach. Surv Geophys. 2013;34(1):121–140.
[31] Canelli L, Ferrero A, Migliazza M, et al. Debris flow risk mitigation by the means of rigid and flexible barriers-experimental tests and impact analysis. Nat Hazard Earth Syst. 2012; 12(5):1693–1699.
[32] Volkwein A, Wendeler C, Guasti G. Design of flexible debris flow barriers. In: Genevois R, Hamilton DL, Prestininzi A, editors. 5th International Conference on Debris-flow Hazard Mitigation: Mech Predic Assess; 2011 Jun 14-17; Padua, Italy; 2011. p. 1093–1100.
[33] Song D, Choi C, Ng C, et al. Geophysical flows impacting a flexible barrier: effects of solid-fluid interaction. Landslides. 2017;15(1):99–110.
[34] Vagnon F, Segalini A. Debris flow impact estimation on a rigid barrier. Nat Hazard Earth Syst. 2016;16(7):1691–1697.
[35] Moriguchi S, Borja RI, Yashima A, et al. Estimating the impact force generated by granular flow on a rigid obstruction. Acta Geotech. 2009;4(1):57–71.
[36] Jiang YJ, Towhata I. Experimental study of dry granular flow and impact behavior against a rigid retaining wall. Rock Mech Rock Eng. 2013;46(4):713–729.
[37] Choi CE, Ng C, Goodwin G, et al. Flume investigation of the influence of rigid barrier deflector angle on dry granular overflow mechanisms. Can Geotech J. 2016;53(10):1751–1759.
[38] Armanini A, Dalri C, Larcher M. Slit-check dams for controlling debris flow and mudflow. In: Marui H, Mikos M, editors. Disaster mitigation of debris flows, slope failures and landslides: proceedings of the interpraevent international symposium; 2006 Sept 25-26; Tokyo, Japan; 2006. p. 141–148.
[39] Choi CE, Law RPH. Performance of landslide debris-resisting baffles. HKIE Transactions. 2015;22(4):235–246.
[40] Fiskum E. Flomskred - testing av ulike sikringstiltak i modellforsøk [master's thesis]. Trondheim, Norway: Norwegian University of Science and Technology (NTNU); 2012.

[41] Le TMH, Christensen SO, Watn A, et al. Effects of deflection wall on run-up height of debris flow. In: Aversa S, Cascini L, Picarelli L, et al., editors. Landslides and Engineered Slopes. Experience, Theory and Practice. CRC Press; 2016. p. 1237–1244.
[42] Gonda Y. Function of a debris-flow brake. Int J of Eros Cont Eng. 2009;2(1):15–21.
[43] Kim Y. Study on hydraulic characteristics of debris flow breakers and sabo dams with a flap [dissertation]. Japan: Kyoto University; 2013.
[44] Xie T, Yang H, Wei F, et al. A new watersediment separation structure for debris flow defense and its model test. B Eng Geol Environ. 2014;73(4):947–958.
[45] Cascini L, Cuomo S, Pastor M, et al. Sph-fdm propagation and pore water pressure modelling for debris flows in flume tests. Eng Geol. 2016;213:74–83.
[46] Fiebiger G. Structures of debris flow countermeasures. In: Chen Cl, editor. Debris-Flow Hazards Mitigation: Mechanics, Prediction, and Assessment; 1997 Aug 7-9; San Francisco (CA). ASCE; 1997. p. 596–605.
[47] NVE. Plan for skredfarekartlegging - delrapport jordskred og flomskred. Norway: NVE - Norwegian Water Resources and Energy Directorate; 2011. Report No. 16/2011.
[48] NPRA. Debris flows and slush avalanches. Norway: Norwegian Public Roads Administration (NPRA); 2016. Handbook V139.
[49] NVE. Preliminary regionalization and susceptibility analysis for landslide early warning purposes in norway. Norway: NVE - Norwegian Water Resources and Energy Directorate; 2014. Report No. 37/2014.
[50] ICHARM. Debris-flow dewatering brakes: a promising tool for disaster management in developing countries. Japan: Public Works Research Institute; 2008. Newsletter 3.
[51] Ochiai H, Sammori T, Okada Y. Landslide experiments on artificial and natural slopes. In: Sassa K, Fukuoka H, Wang F, et al., editors. Progress in landslide science. Berlin, Heidelberg: Springer; 2007. p. 209–226.
[52] Lien HP. Design of slit dams for controlling stony debris flows. Int J Sediment Res. 2003; 18(1):74–87.
[53] ICHARM. Testing and demonstrating a technology to cope with debris flows in mountain regions. The Philippines: International Centre for Water Hazard and Risk Management; 2009. Report.
[54] Savage SB, Iverson RM. Surge dynamics coupled to pore-pressure evolution in debris flows. Debris-Flow Hazards Mitigation: Mech Predict Assess. 2003;1-2:503–514.
[55] Major JJ, Iverson RM. Debris-flow deposition: Effects of pore-fluid pressure and friction concentrated at flow margins. Geol Soc Am Bull. 1999;111(10):1424–1434.
[56] Huebl J, Suda J, Proske D, et al. Debris flow impact estimation. In: Popovska C, editor. International symposium on water management and hydraulic engineering: 2009 Sept 1-5; Ohrid, Macadonia; 2009. p. 137–148.
[57] Laache E. Model testing of the drainage screen type debris flow breaker [master's thesis]. Trondheim, Norway: Norwegian University of Science and Technology (NTNU); 2016.
[58] Watanabe M, Mizuyama T, Uehara S. Review of debris flow countermeasure facilities. J Japan Eros Control Eng Soc. 1980;115:40–45.